Proton MR Spectroscopy and Preoperative Diagnostic Accuracy: An Evaluation of Intracranial Mass Lesions Characterized by Stereotactic Biopsy Findings

Isabella Maria Burtscher, Gunnar Skagerberg, Bo Geijer, Elisabet Englund, Freddy Ståhlberg and Stig Holtås

AJNR Am J Neuroradiol 2000, 21 (1) 84-93
http://www.ajnr.org/content/21/1/84

AJNR Am J Neuroradiol 21:84–93, January 2000

Proton MR Spectroscopy and Preoperative Diagnostic Accuracy: An Evaluation of Intracranial Mass Lesions Characterized by Stereotactic Biopsy Findings

Isabella Maria Burtscher, Gunnar Skagerberg, Bo Geijer, Elisabet Englund, Freddy Ståhlberg, and Stig Holtås

BACKGROUND AND PURPOSE: **MR imaging has made it easier to distinguish among the different types of intracranial mass lesions. Nevertheless, it is sometimes impossible to base a diagnosis solely on clinical and neuroradiologic findings, and, in these cases, biopsy must be performed. The purpose of this study was to evaluate the hypothesis that proton MR spectroscopy is able to improve preoperative diagnostic accuracy in cases of intracranial tumors and may therefore obviate stereotactic biopsy.**

METHODS: **Twenty-six patients with intracranial tumors underwent MR imaging, proton MR spectroscopy, and stereotactic biopsy. MR spectroscopic findings were evaluated for the distribution pattern of pathologic spectra (NAA/Cho ratio $<$ 1) across the lesion and neighboring tissue, for signal ratios in different tumor types, and for their potential to improve preoperative diagnostic accuracy.**

RESULTS: **Gliomas and lymphomas showed pathologic spectra outside the area of contrast enhancement while four nonastrocytic circumscribed tumors (meningioma, pineocytoma, metastasis, and germinoma) showed no pathologic spectra outside the region of enhancement. No significant correlation was found between different tumor types and signal ratios. MR spectroscopy improved diagnostic accuracy by differentiating infiltrative from circumscribed tumors; however, diagnostic accuracy was not improved in terms of differentiating the types of infiltrative or circumscribed lesions.**

CONCLUSION: **MR spectroscopy can improve diagnostic accuracy by differentiating circumscribed brain lesions from histologically infiltrating processes, which may be difficult or impossible solely on the basis of clinical or neuroradiologic findings.**

MR imaging has made it easier to detect and distinguish among intracranial mass lesions. Nevertheless, in some cases, it is impossible to base a specific diagnosis solely on clinical and neuroradiologic findings. Thus, biopsy has to be performed to provide a diagnosis as the basis for treatment regimens. Open biopsy is commonly used, and, if possible, combined with open resection of the intracranial tumor. Lesions located in vital or eloquent parts of the brain, however, may be unsuitable for open neurosurgical intervention.

The purpose of this study was to evaluate the hypothesis that proton MR spectroscopy might be able to improve preoperative diagnostic accuracy in patients scheduled for stereotactic biopsy of intracranial mass lesions and therefore obviate biopsy in some cases.

Methods

Patients

Twenty-six patients, comprising 15 men, 26 to 76 years old, and 11 women, 31 to 80 years old (mean age, 52 years), with a suspected intracranial malignant tumor scheduled for X-ray CT-guided stereotactic biopsy were included in the study. All patients underwent a preoperative workup adapted to the individual's clinical history and situation. All patients had intracranial tumors, which were difficult or impossible to classify solely on the basis of clinical and neuroradiologic findings, and all were unsuitable for open resection or open biopsy owing to their location in vital, eloquent, or deep parts of the brain. Thus, stereotactic biopsy was required to obtain a histopathologic diagnosis.

Received September 12, 1998; accepted after revision August 17, 1999.

From the Departments of Radiology (I.M.B., B.G., F.S., S.H.), Neurosurgery (G.S.), Pathology (E.E.), and Radiation Physics (F.S.), University Hospital, Lund, Sweden.

Supported by grants from the Swedish Medical Research Council, the Swedish Cancer Society, and the Children Cancer Foundation of Sweden.

Address reprint requests to Isabella M. Burtscher, MD, Department of Radiology, University Hospital, S-22185 Lund, Sweden.

CT, MR Imaging, and MR Spectroscopic Measurements

When a patient was scheduled for a CT-guided biopsy, a preoperative MR examination was performed in addition to the CT study necessary for stereotactic biopsy. Preoperative CT scans were obtained on a Toshiba Express scanner with the patient in the stereotactic frame under general anesthesia.

Preoperative MR imaging was performed the same day as the stereotactic biopsy in seven cases, or 1 day (n = 11), 2 days (n = 1), 4 days (n = 4), 8 days (n = 1), 10 days (n = 1), or 15 days (n = 1) before the procedure. These preoperative MR examinations, including MR imaging for anatomic mapping of the tumors, and the proton MR spectroscopic study, were performed on a 1.5-T unit (Magnetom Vision, Siemens, Germany) using a standard circularly polarized head coil and the proton spectroscopy package provided by the manufacturer.

In each patient, sagittal and axial T1-weighted (450–630/14–17 [TR/TE]) spin-echo (SE) MR images, and axial proton density– and T2-weighted (3710/22,90) fast SE MR images were obtained before MR spectroscopy was performed. MR spectroscopy was followed by contrast-enhanced T1-weighted SE MR imaging in the coronal and axial planes. Three series of orthogonal T1-weighted gradient-echo scout images (100/4.8; flip angle, 80°) covering the lesion were used to position the MR spectroscopic measurement volume. Two-dimensional chemical shift imaging (2D-CSI) was performed in all but one patient; the latter was examined with the single-volume spectroscopy (SVS) technique owing to limitations of the examination time in this case. Furthermore, in five patients, SVS was used in addition to 2D-CSI.

For the 2D-CSI technique, a data set was obtained from a selected volume of 18 to 135 cm^3 (minimum, 3 × 4 × 1.5 cm; maximum, 10 × 9 × 1.5 cm) by using an SE sequence with phase-encoding gradients in two directions, automatic shimming, and gaussian water suppression. Measurement parameters used in 2D-CSI were 1500/270(135 in two cases)/2(1 in six cases)(TR/TE/excitations); 16 × 16 phase-encoding steps; 160 × 160-mm field of view; 15-mm section thickness (20 mm in three patients); and 1024 data points. Data sets of 1.5 cm^3 resolution (2.0 cm^3 in three patients) were acquired within 12 minutes (6 minutes in the six measurements with one excitation).

For the SVS technique, data from cubic volumes of 1.5 × 1.5 × 1.5–2.0 × 2.0 × 2.0 cm were obtained with an SE sequence of 1500/270/128–256; 240 × 240-mm field of view; 1024 data points; and an acquisition time of 3 to 6 minutes, depending on the number of excitations.

Stereotactic Biopsy and Histopathologic Classification

Stereotactic biopsy was performed under general anesthesia immediately after the CT study, except for those seven cases in which MR imaging and MR spectroscopy were performed after CT and before biopsy. The Leksell stereotactic system (Elekta, Stockholm) was used. Target points were chosen on the basis of CT and MR imaging findings.

The tumor types were histopathologically classified according to WHO criteria and afterward divided into five groups (Table 1): low-grade astrocytomas (astrocytoma grade II); high-grade astrocytomas (anaplastic astrocytoma grade III, and glioblastoma multiforme grade IV); lymphomas; miscellaneous nonastrocytic circumscribed tumors; and unclear cases (equivocal histopathologic diagnosis).

Evaluation of MR Spectroscopy

Postprocessing in the time domain included apodization with a gaussian filter and a frequency shift correction followed by Fourier transformation. In the frequency domain, the phase relations within spectra were adjusted and, if necessary, the baseline was straightened by a matching polynomial function.

TABLE 1: List of histopathologic diagnoses

Tumor Type	No.
Low-grade astrocytoma	4
High-grade astrocytoma	13
Lymphoma	4
Miscellaneous nonastrocytic circumscribed tumors (metastasis, germinoma, meningeoma, pineocytoma)	4
Unclear case	1

TABLE 2: Distribution Pattern of pathologic spectra

Diagnosis	No. (No. of Cases Not Evaluated)*	No. of Cases with Pathologic Spectra: Limited to Contrast Enhancement Area	No. of Cases with Pathologic Spectra: Outside Contrast Enhancement Area
Infiltrating lesions:			
Low-grade astrocytoma	4 (1)	0	3
High-grade astrocytoma	13 (3)	0	10
Lymphoma	4 (1)	0	3
Circumscribed lesions:			
Meningioma	1 (0)	1	0
Pineocytoma	1 (0)	1	0
Metastasis	1 (0)	1	0
Germinoma	1 (0)	1	0

Note.—Different tumor types show varying distribution patterns of pathologic spectra and might therefore offer the possibility of differential diagnosis by MR spectroscopy. Spectra were defined as pathologic when NAA/Cho was less than 1/1.

* Number of cases that could not be evaluated for these parameters owing to poor quality of the spectra of interest (n = 3), a voxel positioned outside the lesion (n = 1), or examination with the single-volume spectroscopy technique (n = 1).

MR spectroscopic results were evaluated for the distribution of pathologic spectra across the lesion and neighboring neuroradiologically normal-appearing tissue and for signal ratios in different tumor types. Spectra were defined as pathologic when the ratio of *N*-acetylaspartate/choline-containing compounds (NAA/Cho) was less than 1. Distribution patterns of pathologic spectra were classified in two groups: those limited to the region corresponding to the contrast enhancement, and those outside the region corresponding to the contrast enhancement.

The patient examined only with SVS was excluded from the evaluation of distribution patterns of abnormal spectra, as SVS does not allow one to take the heterogeneity of tumors and neighboring tissue into account.

Substances of interest regarding the calculation of signal ratios in different tumor types were as follows: NAA, 2.0 ppm; Cho, 3.2 ppm; creatine and phosphocreatine (Cr), 3.0 ppm; lipid-containing compounds and/or lactate (Lip-Lac), 0.9 to 1.3 ppm. Signal ratios were calculated for NAA/Cho, NAA/Cr, Cr/Cho, and, if possible, for Lip-Lac/Cho and Lip-Lac/Cr. These ratios were determined for spectra in neuroradiologically normal-appearing tissue of the contralateral hemisphere and in the stereotactic target point in infiltrative tumors (gliomas and lymphomas) in each patient. Metabolite ratios are not presented for circumscribed tumors, since this group was only represented by one patient for each diagnosis.

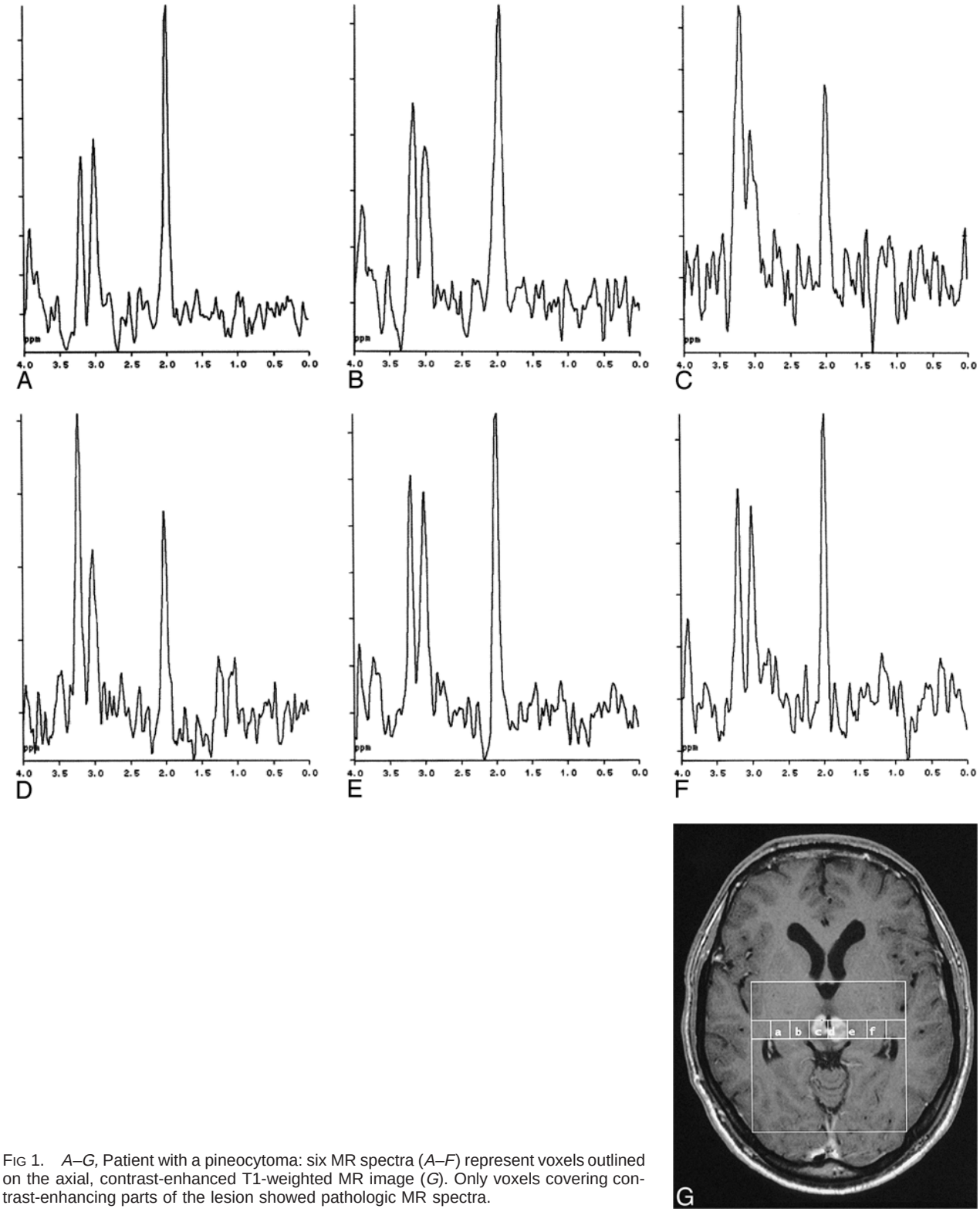

FIG 1. *A–G,* Patient with a pineocytoma: six MR spectra (*A–F*) represent voxels outlined on the axial, contrast-enhanced T1-weighted MR image (*G*). Only voxels covering contrast-enhancing parts of the lesion showed pathologic MR spectra.

To calculate metabolite ratios, a curve-fitting routine was used. An ideal peak function was matched to each peak of interest in the measured spectrum, and, further, the integrated area under each ideal peak, representing the amount of the substance within the volume of interest (VOI), was calculated. Only spectra with a clean baseline and narrow, visually distinct peaks were used for the metabolite ratio calculation. Measurements performed with a TE of 135 were excluded from the calculation of metabolite ratios, although the influence on signal intensity of a decrease of TE from 270 to 135 is most likely of little significance in our data, as they are only semiquantitative.

Evaluation of the Contribution of MR Spectroscopy to Preoperative Diagnostic Accuracy

Analysis of the material was made retrospectively by a neurosurgeon, a neuroradiologist, and a spectroscopist, all blinded to the final histopathologic diagnosis. Each of the observers suggested a reasonable set of differential diagnoses based on preoperative findings as described below. The three observers considered the suggested differential diagnoses to be definite, probable, possible, not probable, or excluded. A preoperative diagnosis was ranked as definite when all other proposed differential diagnoses could definitely be excluded (excluded); it was ranked as probable when other proposed diagnoses were much less probable (not probable) or could definitely be excluded (excluded). When none of the suggested differential diagnoses could be ranked definite or probable and two or more diagnoses seemed equally possible, the preoperative diagnosis was ranked as possible. Diagnoses not suggested by the observers in the ranking were defined as excluded.

The preoperative differential diagnoses of the neuroradiologist were based on all neuroradiologic material available at the time of stereotactic biopsy, including MR imaging but excluding MR spectroscopic results, and on the clinical information included in the requisitions. The neurosurgeon based his preoperative diagnoses on information from the patients' records, including all neuroradiologic reports with the exception of MR spectroscopic results. On the basis of spectral and distribution patterns of the pathologic spectra seen at MR spectroscopy, the spectroscopist reevaluated and ranked the preoperative diagnoses proposed by the neuroradiologist.

The proposed diagnoses of the three observers were compared with histopathologic findings, and their accuracy was evaluated by comparing a) the number of correctly ranked differential diagnoses for each observer, and b) the percentage of correct diagnoses for the three observers. A correct definite, probable, possible, not probable, or excluded diagnosis accounted for 100%, 75%, 50%, 25%, or 0% correct diagnoses, respectively. Hence, MR spectroscopic results could be evaluated as to their potential to improve preoperative diagnostic accuracy by comparing the number of correctly ranked differential diagnoses and the percentage of correct diagnoses of the spectroscopist as compared with the other two observers. For statistical evaluation, the Mann-Whitney U test and Fisher's exact test were used. *P* values less than .05 were considered significant.

Results

The tumor types investigated are shown in Table 1. Seventeen of 26 specimens represented gliomas, four were lymphomas, and four were miscellaneous nonastrocytic circumscribed tumors, whereas the last case remained unclear.

When comparing the MR spectroscopic results as to distribution patterns of pathologic spectra against the histopathologic findings, all gliomas and lymphomas showed pathologic spectra outside the area of contrast enhancement (Table 2). The four circumscribed lesions, including a meningioma, a pineocytoma (Fig 1), a metastasis of adenocarcinoma, and a germinoma, showed no pathologic spectra outside the region of contrast enhancement. In addition, gliomas (Fig 2) showed pathologic spectra outside the neuroradiologically defined lesion in all cases in which VOI sizes allowed an evaluation of normal-appearing tissue close to the lesion. The distribution pattern of pathologic spectra could not be evaluated in five patients owing to poor spectral quality (n = 3), to a VOI not covering the biopsy target point (n = 1), or to only a single SVS measurement being taken (n = 1).

No significant correlation was found between signal ratios representing tissue from the target point of the stereotactic biopsy and different tumor types (low-grade and high-grade astrocytomas and lymphomas) (Table 3 and Fig 3). Figure 4 shows MR spectroscopic scout images and spectra representing the target points in a high-grade and a low-grade astrocytoma, the spectra being almost identical. Signal ratios from the stereotactic biopsy target point could not be calculated in two patients owing to poor spectral quality and in one patient owing to a VOI not covering the target point.

With respect to the question of infiltrative versus circumscribed tumor, a consideration of the distribution pattern of pathologic spectra led in five cases to a higher level of preoperative diagnostic accuracy as compared with the neuroradiologic diagnosis (Table 4). Improved diagnostic accuracy by MR spectroscopy was noted in three high-grade astrocytomas that were neuroradiologically interpreted as metastases, and in one case as possible metastasis or glioma; in an adenocarcinoma metastasis (neuroradiologic diagnosis: high-grade astrocytoma); and in a lymphoma (neuroradiologic diagnosis: abscess).

The increase in diagnostic accuracy varied between one rank (probable → definite) and four ranks (excluded → definite). Cases with decreased diagnostic accuracy were not found in the group of differential diagnoses of infiltrative versus circumscribed lesions. Nevertheless, a lower diagnostic accuracy as compared with the neuroradiologic diagnoses was seen in the differential diagnosis between different infiltrative lesions (n = 4) and between different circumscribed lesions (n = 1) (Table 4). The decrease in accuracy in these two groups varied between one rank (definite → probable; probable → possible) and two ranks (definite → possible). In these cases, as compared with the group of differential diagnoses of infiltrative versus circumscribed lesions, MR spectroscopy cannot contribute to the differential diagnosis by means of distribution patterns of pathologic spectra.

Table 5 gives the preoperative diagnostic accuracy in terms of the number of cases with correctly ranked (true) differential diagnoses (definite, probable, possible, not probable, and excluded) for each observer, and the total percentage of correct diagnoses for the three observers. MR spectroscopy showed a slightly higher percentage of correct diagnoses as compared with the other observers, but the difference was not statistically significant (Fisher's exact test). It is noteworthy that diagnoses ranked definite or probable by MR spectroscopic findings were in all cases true when

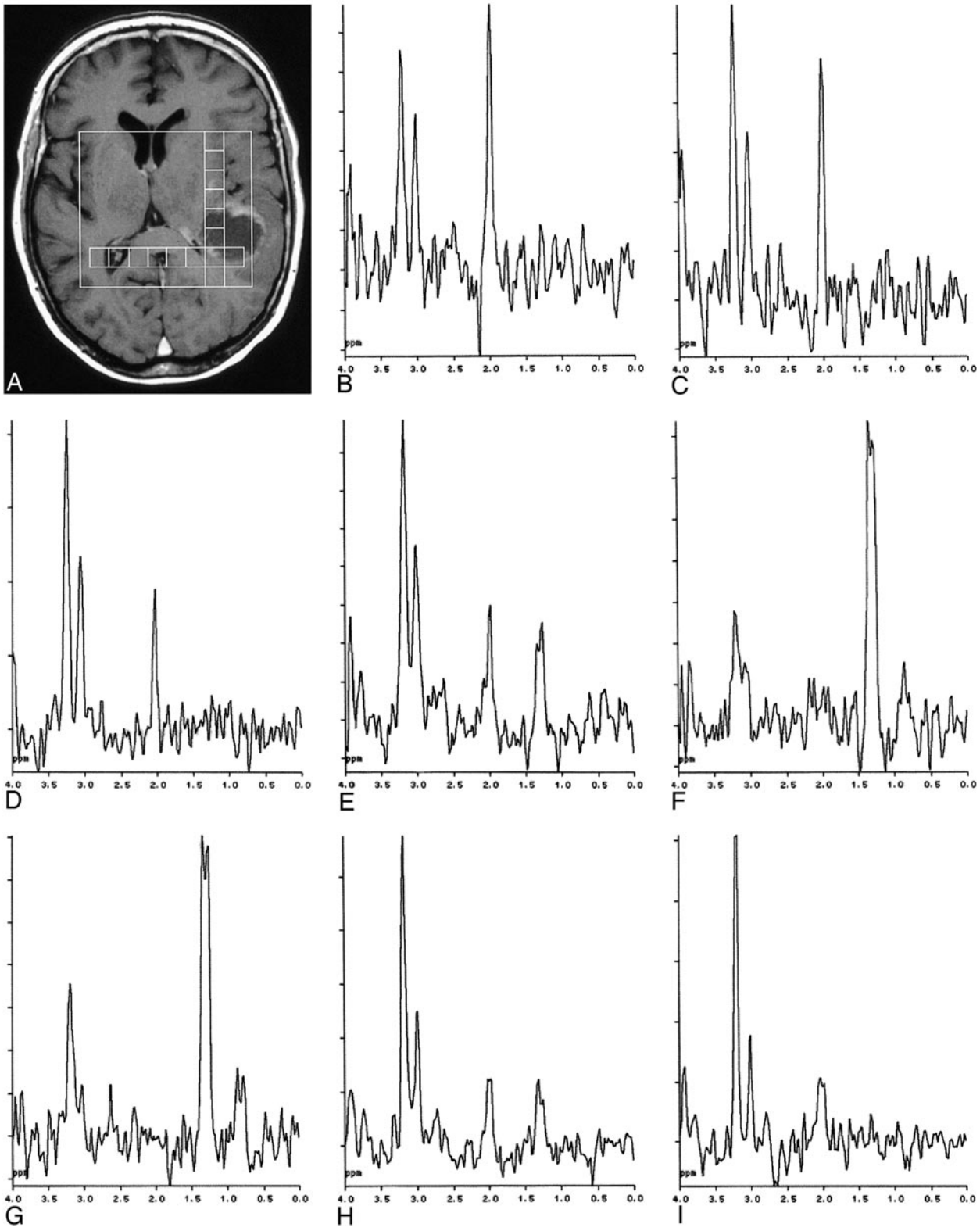

compared with histopathologic findings, whereas for both the neuroradiologically and clinically based diagnoses, false-definite and false-probable rankings occurred.

Discussion

In the clinical setting, diagnosis of intracranial mass lesions can be complicated by ambiguous

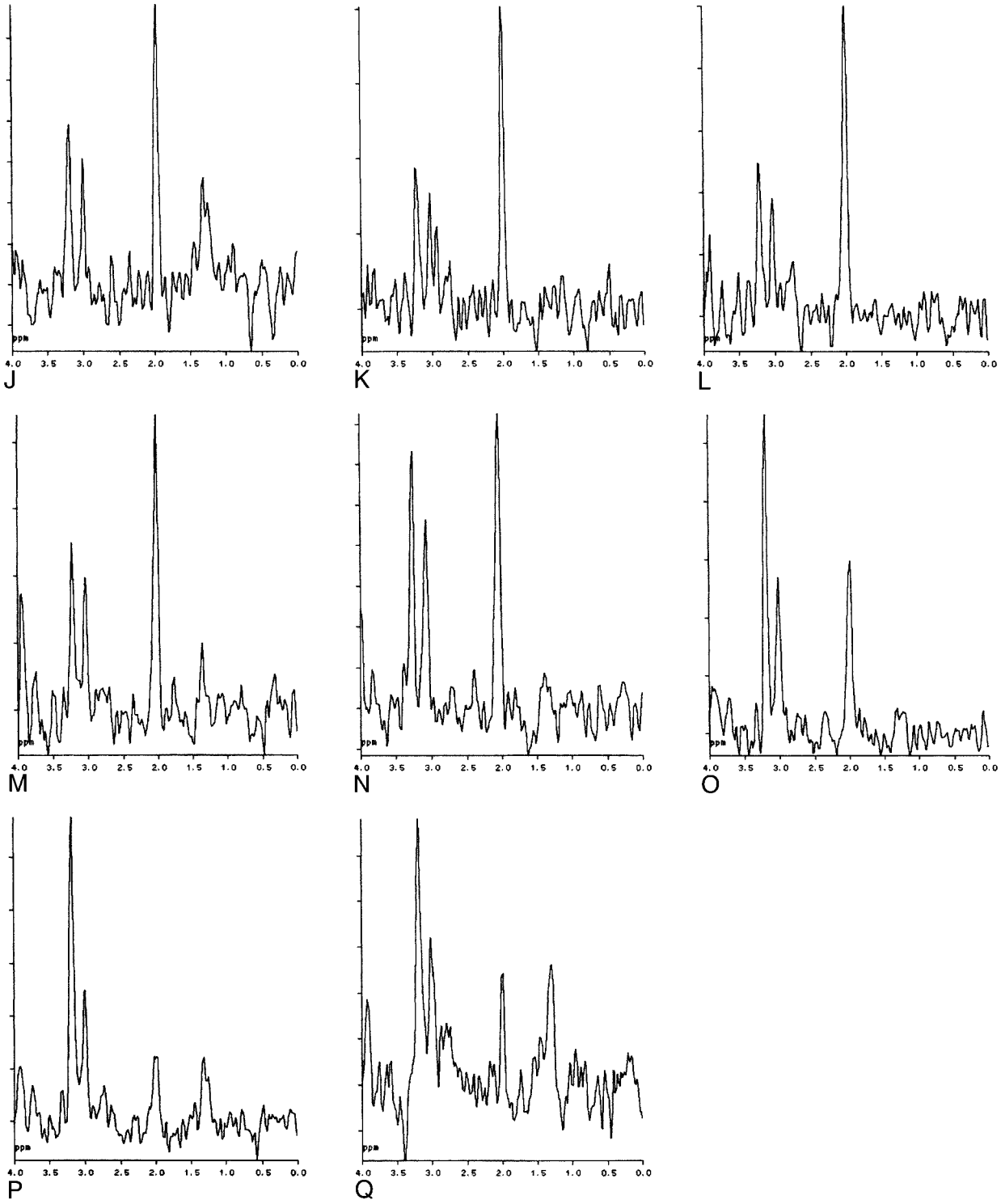

← FIG 2. *A–Q,* Patient with a cystic high-grade glioma: the images show the heterogeneity of spectra across the lesion. *A* is an axial, contrast-enhanced T1-weighted MR image with the measurement area and voxels represented by the MR spectra in *B–Q* outlined; *B–I* represent voxels in the vertical row (*top to bottom*) and (*J–Q*) represent voxels in the horizontal row (*left to right*). The spectrum representing the intersection of the vertical and horizontal rows is shown twice (*H* and *P*).

neuroradiologic findings, uncharacteristic clinical symptoms or symptom onset. In these cases, additional diagnostic methods are solicited, and MR spectroscopy might, at least when dealing with some specific diagnostic problems, be able to increase diagnostic accuracy by adding another piece to the diagnostic puzzle. When discussing spectroscopic data of brain lesions, the significance of calculation of signal ratios and the use of these ratios for determining the degree of tumor malignancy or for characterizing histologic tumor types or subtypes is often stressed (1–16). Published findings are

TABLE 3: Signal ratios in neuroradiologically normal-appearing tissue and in the stereotactic target point (mean ± SD)

Tissue Type	No.	NAA/Cho	NAA/Cr	Cr/Cho	Lip-Lac/Cho	Lip-Lac/Cr
Normal tissue	14	2.18 ± 0.37	2.41 ± 0.39	0.92 ± 0.19	. . .	. . .
Low-grade astrocytoma	4	0.48 ± 0.42	1.33 ± 0.82	0.32 ± 0.12	0.41 ± 0.15	1.41 ± 0.54
High-grade astrocytoma	11*	0.51 ± 0.39	0.99 ± 0.59	0.49 ± 0.23	0.87 ± 1.01	3.34 ± 5.10
Lymphoma	3†	0.94 ± 0.52	1.46 ± 0.51	0.61 ± 0.13	2.92 ± 2.96	5.35 ± 6.24

Note.—Signal ratios calculated for neuroradiologically normal-appearing tissue of the contralateral hemisphere differed significantly from sig nal ratios calculated for tumor tissue; however, no significant correlation was found between signal ratios and different tumor types. Signal ratios in tumor tissue represent stereotactic biopsy target points. NAA indicates *N*-acetylaspartate; Cho, choline-containing compounds; Cr, creatine and phosphocreatine; Lip-Lac, and lipid-containing compounds or lactate or both.

* Two of the 13 patients with high-grade gliomas could not be evaluated owing to poor quality.

† One patient with a lymphoma could not be evaluated because the volume of interest did not cover the lesion and a TE of 135 was used.

contradictory, however, and some authors point out that the spectral signatures of brain tumors correlate imperfectly with their histologic diagnosis (1–6). Our results support the lack of correlation between different tumor types and signal ratios from measurements in the stereotactic target point (Table 3). Recent studies based on neural network analysis and automated pattern recognition—for example, Preul et al (15)—showed promising results regarding the classification of brain tumors. Applying these statistical methods in the clinical situation, however, is difficult because a) large learning data sets are required, b) only tumor groups well represented in the learning set can be analyzed properly, and c) clinical and radiologic information can be difficult to implement in the analysis.

When analyzing spectra from CSI measurements for signal ratios and the regional distribution of pathologic spectra across the lesion, it becomes obvious that the latter might have a great impact for clinical cases in which differentiating infiltrating from circumscribed tumors or from tumor-like lesions is difficult. As presented in Table 2, infiltrative and circumscribed lesions show varying distribution patterns of pathologic MR spectra. Our results suggest that tumor infiltration beyond the area of contrast enhancement or beyond the margins of neuroradiologically obvious tumor in patients with high-grade gliomas is disclosed on MR spectroscopy as pathologic spectra with NAA/Cho ratios of less than 1. A comparable widespread infiltrative pattern is often seen histopathologically in cases of high-grade gliomas (17, 18).

Edema, often seen surrounding brain lesions, does not, to our knowledge, cause spectral abnormalities as severe as those seen in gliomas. Circumscribed lesions such as meningiomas, metastases, or abscesses only rarely show histopathologic infiltration of neighboring tissue, and, to our knowledge, are not reported to show abnormal spectra with NAA/Cho ratios of less than 1 outside the lesion. A differential diagnosis between different circumscribed lesions based on varying spatial distribution patterns of pathologic spectra does not, therefore, appear to be possible from our data. In this situation, however, evaluation of the occurrence of special metabolites and their signal intensities might help to differentiate various circumscribed lesions from one other, as

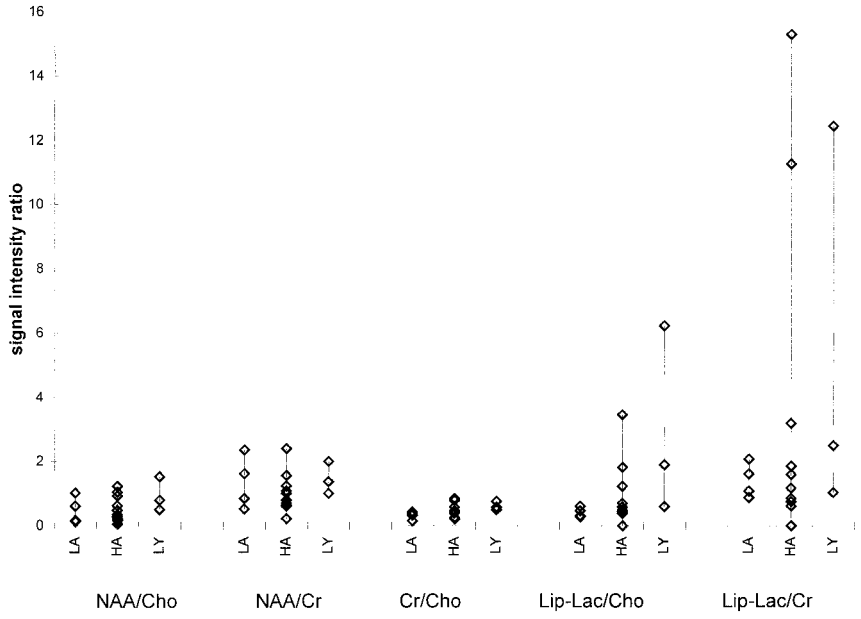

FIG 3. Scattergram of signal ratios in stereotactic biopsy target points for different tumor types. *LA* = low-grade astrocytoma (n = 4), *HA* = high-grade astrocytoma (n = 11), *LY* = lymphoma (n = 3).

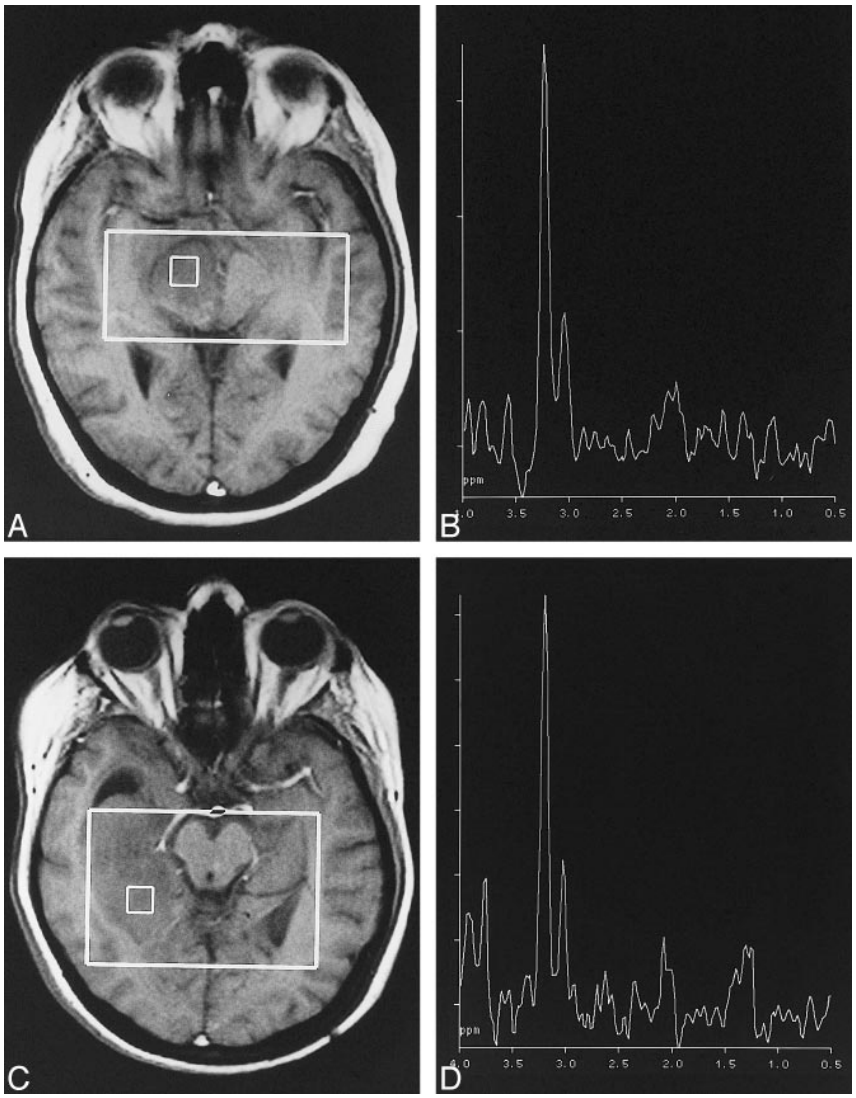

FIG 4. MR spectroscopic scout images and corresponding spectra represent the stereotactic biopsy target points in a high-grade (*A* and *B*) and a low-grade (*C* and *D*) astrocytoma. The two spectra are almost identical, and signal ratios could not be used to grade the tumors.

has been suggested for abscesses (12, 19–22) or meningiomas (2, 3, 6, 7, 12, 23, 24). As histopathology still represents the standard of reference in diagnostic classification of intracranial gliomas and other brain tumors, the main advantage of MR spectroscopy at the moment is its potential as a possible instrument for a noninvasive differential diagnosis between infiltrative tumors versus circumscribed lesions as metastases and abscesses. This, however, has to be proved further in larger studies evaluating MR spectroscopy in the clinical practice.

The first prerequisite for evaluation of regional spectral patterns in intracranial mass lesions is to measure as many parts across a lesion and its neighboring tissue as possible within a time frame as short as possible. With chemical shift imaging, this becomes partly possible (9, 25), and it is hoped that, in the future, clinically available multislice spectroscopic imaging combined with better spatial resolution will make it even easier.

Apart from the possibility of increasing diagnostic confidence in patients with intracranial mass lesions, MR spectroscopy also was helpful in guiding the stereotactic biopsy. Based on Lac and Lip-containing compounds often seen in necrotic parts of mass lesions, MR spectroscopy might be used to differentiate between physiologically active and inactive or necrotic parts of lesions. Furthermore, pathologic levels of Cho and pathologic NAA/Cho ratios in neuroradiologically normal-appearing tissue can reveal locations that could be used as target points for the stereotactic biopsy with less risk. The identification of alternative target points becomes essential for the neurosurgeon when the contrast-enhancing target is located in an eloquent brain region or is difficult to approach safely by stereotactic biopsy. Guidance of the stereotactic biopsy by means of MR spectroscopy might also reduce the number of biopsies performed in individual patients with lesions difficult to classify and, hence, decrease the risk for complications associated with the stereotactic procedure (26).

TABLE 4: Influence of MR spectroscopy on diagnostic accuracy as compared with neuroradiologic diagnosis based on distribution pattern of pathologic spectra

Differential Diagnosis	No. of Cases		
	Increased Accuracy	Unchanged Accuracy	Decreased Accuracy
Infiltrative versus circumscribed lesions	5	1 + 1* + 1†	0
Between different infiltrative lesions	0	6 + 1‡ + 2† + 2§	4
Between different circumscribed lesions	0	1§	1

Note.—With respect to the question of infiltrative versus circumscribed tumor, a consideration of the distribution pattern of pathologic spectra led in five cases to a higher level of preoperative diagnostic accuracy as compared with the neuroradiologic diagnosis. A lower diagnostic accuracy relative to the neuroradiologic diagnoses was, however, found between different infiltrative lesions (n = 4) and between different circumscribed lesions (n = 1). The distribution pattern of pathologic spectra outside the area of contrast enhancement could not be interpreted * because the volume of interest (VOI) was positioned outside the lesion, or † because of poor quality or a lack of neuroradiologically normal-appearing tissue in the VOI, or ‡ because only single-volume spectroscopy was performed. § MR spectroscopy confirmed a proposed single diagnosis.

TABLE 5: Number of cases with true, histopathologically verified diagnoses for the different observers and different ranks

Rank of Preoperative Diagnosis	Neuroradiologist	Spectroscopist	Neurosurgeon
Definite	5 of 6	7 of 7	7 of 8
Probable	8 of 9	3 of 3	9 of 14
Possible	8 of 10	12 of 12	3 of 3
Not probable	5 of 6	1 of 1	11 of 13
Excluded	1 of 1	4 of 4	0 of 0
Percentage of (no.) true diagnoses	60 (25)	69 (22)*	61 (25)

Note.—The preoperative diagnostic accuracy is given in terms of the number of cases with correctly ranked (true) differential diagnoses for each observer, and the percentage of correct diagnoses for the three observers, where a correct definite, probable, possible, not probable, or excluded diagnosis accounted for 100%, 75%, 50%, 25%, or 0% of cases, respectively. Hence, 100% correct diagnoses would require exclusively true definite diagnoses. When interpreting this table it has to be taken into account that one patient usually had more than one preoperative differential diagnosis and that the sum of the numbers in the vertical direction therefore is not equal to the number of evaluated patients.

* In three patients, MR spectroscopic results were not of sufficient quality to rank the preoperative differential diagnoses proposed by the neuroradiologist and were therefore excluded.

Conclusion

Based on the distribution of pathologic spectra across brain lesions, MR spectroscopy can improve diagnostic accuracy in the differentiation of circumscribed brain lesions from histologically infiltrating processes, which is often difficult or impossible by conventional morphologic methods. Such a differentiation is of potential clinical importance, since in circumscribed lesions, surgery might be curative whereas infiltrative lesions, especially in eloquent areas, are generally better handled by other treatment methods, such as irradiation or chemotherapy. On the other hand, while MR spectroscopy might not help in differentiating the various infiltrative lesions, it may provide valuable support to MR imaging in detecting and selecting an appropriate target point for stereotactic biopsy in these cases.

Acknowledgments

We express our gratitude to our colleagues in the Departments of Diagnostic Radiology and Neurosurgery, University Hospital Lund, Sweden.

References

1. Demaerel P. ***In vivo* localized single-voxel proton magnetic resonance spectroscopy of intracranial tumors.** *Int J Neuroradiol* 1997;3:94–110
2. Henriksen O, Wieslander S, Gjerris F, Jensen KM. **In vivo ^{1}H-spectroscopy of human intracranial tumors at 1.5 Tesla: preliminary experience at a clinical installation.** *Acta Radiol* 1991; 32:95–99
3. Demaerel P, Johannik K, Van Hecke P, et al. **Localized ^{1}H NMR spectroscopy in fifty cases of newly diagnosed intracranial tumors.** *J Comput Assist Tomogr* 1991;15:67–76
4. Sutton LN, Wehrli SL, Gennarelli L, et al. **High-resolution ^{1}H-magnetic resonance spectroscopy of pediatric posterior fossa tumors *in vitro*.** *J Neurosurg* 1994;81:443–448
5. Sijens PE, Knopp MV, Brunetti A, et al. **^{1}H MR spectroscopy in patients with metastatic brain tumors: a multicenter study.** *Magn Reson Med* 1995;33:818–826
6. Ott D, Henning J, Ernst T. **Human brain tumors: assessment with in vivo proton MR spectroscopy.** *Radiology* 1993;186:745–752
7. Poptani H, Gupta RK, Roy R, Pandey R, Jain VK, Chhabra DK. **Characterization of intracranial mass lesions with in vivo proton MR spectroscopy.** *AJNR Am J Neuroradiol* 1995;16:1593–1603
8. Shimizu H, Kumabe T, Tominaga T, et al. **Nonivasive evaluation of malignancy of brain tumors with proton MR spectroscopy.** *AJNR Am J Neuroradiol* 1996;17:737–747
9. Tzika AA, Vajapeyam S, Barnes PD. **Multivoxel proton MR spectroscopy and hemodynamic MR imaging of childhood brain tumors: preliminary observations.** *AJNR Am J Neuroradiol* 1997;18:203–218
10. Usenius J-PR, Kauppinen RA, Vainio PA. **Quantitative metabolite patterns of human brain tumors: detection by ^{1}H NMR spectroscopy in vivo and in vitro.** *J Comput Assist Tomogr* 1994; 18:705–713
11. Arle JE, Morriss C, Wang ZJ, Zimmerman RA, Phillips PG, Sutton LN. **Prediction of posterior fossa tumor type in children by means of magnetic resonance image properties, spectroscopy, and neural networks.** *J Neurosurg* 1997;86:755–761
12. Poptani H, Gupta RK, Jain VK, Roy R, Pandey R. **Cystic intracranial mass lesions: possible role of in vivo MR spectroscopy in its differential diagnosis.** *Magn Reson Imaging* 1995;13:1019–1029
13. Sijens PE, van den Bent MJ, Nowak PJCM, van Dijk P, Oudkerk M. **^{1}H chemical shift imaging reveals loss of brain tumor choline signal after administration of GD-contrast.** *Magn Reson Med* 1997;37:222–225
14. Laws ER. **Imaging brain tumors: beyond three dimensions.** *Nat Med* 1996;2:271–272
15. Preul MC, Caramanos Z, Collins DL, et al. **Accurate, noninvasive diagnosis of human brain tumors by using proton magnetic resonance spectroscopy.** *Nat Med* 1996;2:323–325
16. Barkovich AJ. **Brain tumors of childhood.** In: *Pediatric Neuroimaging.* 2nd ed. New York: Raven; 1995:338–340
17. Scheithauer BW. **The forms of growth in gliomas and their practical significance.** *Brain* 1940;63:1–35
18. Burger PC. **Classification, grading and patterns of spread of malignant gliomas.** In: Apuzzo ML, ed. *Neurosurgical Topics: Malignant Cerebral Glioma.* Park Ridge, IL: American Association of Neurological Surgeons; 1990:3–17

19. Martinez-Pérez I, Moreno Á, Alonso J, et al. **Diagnosis of brain abscess by magnetic resonance spectroscopy.** *J Neurosurg* 1997;86:708–713
20. Harada M, Tanouchi M, Miyoshi H, Nishitani H, Kannuki S. **Brain abscess observed by localized proton magnetic resonance spectroscopy.** *Magn Reson Imaging* 1994;12:1269–1274
21. Rémy C, Grand S, Lai ES, et al. **1H MRS of human brain abscesses in vivo and in vitro.** *Magn Reson Med* 1995;34:508–514
22. Kim SH, Chang K-H, Song IC, et al. **Brain abscess and brain tumor: discrimination with in vivo H-1 MR spectroscopy.** *Radiology* 1997;204:239–245
23. Chang Yue N. **Advances in brain tumor imaging.** *Curr Opin Neurol* 1993;6:831–840
24. Florian CL, Preece NE, Bhakoo KK, Williams SR, Noble MD. **Cell type-specific fingerprinting of meningioma and meningeal cells by proton nuclear magnetic resonance spectroscopy.** *Cancer Res* 1995;55:420–427
25. Vigneron DB, Nelson SJ, Myrphy-Boesch J, et al. **Chemical shift imaging of human brain: axial, sagittal, and coronal P-31 metabolite images.** *Radiology* 1990;177:643–649
26. Blaauw G, Braakman R. **Pitfalls in diagnostic stereotactic brain surgery.** *Acta Neurochir* 1988;42(Suppl):161–165